AMERICAN SOCIETY FOR MICROBIOLOGY | Journal of Virology®

VIRUS-CELL INTERACTIONS

Porcine Hemagglutinating Encephalomyelitis Virus Activation of the Integrin $\alpha5\beta1$-FAK-Cofilin Pathway Causes Cytoskeletal Rearrangement To Promote Its Invasion of N2a Cells

Xiaoling Lv,[a] Zi Li,[a] Jiyu Guan,[a] Shiyu Hu,[a] Jing Zhang,[a] Yungang Lan,[a] Kui Zhao,[a] Huijun Lu,[b] Deguang Song,[a] Hongbin He,[c] Feng Gao,[a] Wenqi He[a]

[a]Key Laboratory of Zoonosis Research, Ministry of Education, College of Veterinary Medicine, Jilin University, Changchun, China
[b]Key Laboratory of Zoonosis Research, Ministry of Education, Institute of Zoonosis, Jilin University, Changchun, China
[c]College of Life Sciences, Shandong Normal University, Jinan, China

ABSTRACT Porcine hemagglutinating encephalomyelitis virus (PHEV) is a highly neurotropic virus that causes diffuse neuronal infection with neurological damage and high mortality. Virus-induced cytoskeletal dynamics are thought to be closely related to this type of nerve damage. Currently, the regulation pattern of the actin cytoskeleton and its molecular mechanism remain unclear when PHEV enters the host cells. Here, we demonstrate that entry of PHEV into N2a cells induces a biphasic remodeling of the actin cytoskeleton and a dynamic change in cofilin activity. Viral entry is affected by the disruption of actin kinetics or alteration of cofilin activity. PHEV binds to integrin $\alpha5\beta1$ and then initiates the integrin $\alpha5\beta1$-FAK signaling pathway, leading to virus-induced early cofilin phosphorylation and F-actin polymerization. Additionally, Ras-related C3 botulinum toxin substrate 1 (Rac1), cell division cycle 42 (Cdc42), and downstream regulatory gene p21-activated protein kinases (PAKs) are recruited as downstream mediators of PHEV-induced dynamic changes of the cofilin activity pathway. In conclusion, we demonstrate that PHEV utilizes the integrin $\alpha5\beta1$-FAK-Rac1/Cdc42-PAK-LIMK-cofilin pathway to cause an actin cytoskeletal rearrangement to promote its own invasion, providing theoretical support for the development of PHEV pathogenic mechanisms and new antiviral targets.

IMPORTANCE PHEV, a member of the *Coronaviridae* family, is a typical neurotropic virus that primarily affects the nervous system of piglets to produce typical neurological symptoms. However, the mechanism of nerve damage caused by the virus has not been fully elucidated. Actin is an important component of the cytoskeleton of eukaryotic cells and serves as the first obstacle to the entry of pathogens into host cells. Additionally, the morphological structure and function of nerve cells depend on the dynamic regulation of the actin skeleton. Therefore, exploring the mechanism of neuronal injury induced by PHEV from the perspective of the actin cytoskeleton not only helps elucidate the pathogenesis of PHEV but also provides a theoretical basis for the search for new antiviral targets. This is the first report to define a mechanistic link between alterations in signaling from cytoskeleton pathways and the mechanism of PHEV invading nerve cells.

KEYWORDS cofilin, porcine hemagglutinating encephalomyelitis virus, coronavirus, cytoskeletal rearrangement, integrin $\alpha5\beta1$, neurotropic virus

The cytoskeleton is a network of fibers in eukaryotic cells that are involved in maintaining cell morphology and cell motility, including microtubules, microfilaments (also known as actin filaments), and intermediate filaments (1). Although a virus does not contain a cytoskeletal system, viruses utilize the cytoskeleton system of a host

Citation Lv X, Li Z, Guan J, Hu S, Zhang J, Lan Y, Zhao K, Lu H, Song D, He H, Gao F, He W. 2019. Porcine hemagglutinating encephalomyelitis virus activation of the integrin α5β1-FAK-cofilin pathway causes cytoskeletal rearrangement to promote its invasion of N2a cells. J Virol 93:e01736-18. https://doi.org/10.1128/JVI.01736-18.

Editor Julie K. Pfeiffer, University of Texas Southwestern Medical Center

Address correspondence to Wenqi He, hewq@jlu.edu.cn.

X.L. and Z.L. contributed equally to this article.

Received 2 October 2018
Accepted 5 December 2018
Accepted manuscript posted online 12 December 2018
Published 19 February 2019

cell to complete the infection process (2, 3). Currently, numerous experiments show that the actin cytoskeleton is crucial for many stages of the viral life cycle, including binding, entry, nuclear localization, genomic transcription and reverse transcription, assembly, and export/dissemination (4–6). Porcine hemagglutinating encephalomyelitis virus (PHEV), a member of the *Coronaviridae* family, is a highly neurovirulent virus that spreads to the central nervous system via peripheral nerves (7). Pig is the natural host of PHEV, but the virus has been adapted to replicate in mouse and mouse neuroblastoma N2a cells (N2a cells) (8). PHEV infection induces neurite damage and neuronal death, which may be the cause of neurological symptoms (9). Moreover, PHEV also utilizes the host actin-related protein CASK interacting protein 1 (Caskin1) to facilitate replication of the virus in host cells (10). Studying the mechanism of PHEV entry into the cell from the perspective of the interaction between virus infection and host actin cytoskeleton has great scientific significance for exploring pathogenesis and developing new antiviral drugs.

The first obstacle encountered by virus-infected cells is the cortical actin cytoskeleton, which is located below the plasma membrane and consists of a network of loosely organized fibrous actin (F-actin) (4). The dynamics of the actin cytoskeleton play an important role in the maintenance of cell morphology and in preventing the invasion of pathogens (11). This dynamic change includes the formation of various actin scaffolds of filopodia, lamellipods, and stress fibers as well as other functions, which are regulated by the activation of their upstream signaling pathways in which the small G protein family Rho GTPases plays a crucial role (12). Many pathogens, including viruses, facilitate their entry into and/or trafficking in cells by stimulating actin cytoskeleton remodeling (13). Furthermore, effective virus entry is achieved by induction of actin remodeling (14, 15). The most commonly utilized members of the Rho GTPases for viruses are the ras homolog gene family, including member A (RhoA), Ras-related C3 botulinum toxin substrate 1 (Rac1), and cell division cycle 42 (Cdc42) (16). For example, RhoA and Rac1 GTPase-mediated actin cytoskeletal rearrangements during Japanese encephalitis virus (JEV) infection are crucial for viral endocytosis (16). Cofilin is an important regulatory protein of the cytoskeletal depolymerization factor family and is widely involved in cell migration, among other processes (17). LIM kinase (LIMK) inhibits cofilin activity by phosphorylating serine residue 3 (Ser-3). LIMK can be activated by Rho-associated kinase (ROCK), which is a downstream kinase of RhoA, and p21-activated protein kinases (PAKs), which are downstream kinases of Rac1 and Cdc42 (18). Integrins, a large family of transmembrane glycoproteins, play an important role in the regulation of various cellular functions. Many pathogens use integrin to regulate cytoskeletal functions to promote infection (19, 20). Activation of focal adhesion kinase (FAK), which is a key tyrosine kinase in the integrin signaling pathway, activates Rac1 and Cdc42 (21). PHEV enters N2a cells through clathrin-mediated endocytosis, and this process leads to a rapid rearrangement of actin (22), but the role of actin rearrangement and the molecular mechanisms responsible for its action remain unclear.

In this study, we studied the morphological changes of the actin cytoskeleton during the entry of PHEV into N2a cells and its mechanism. The results showed that dynamic changes in cofilin activity affected viral infection. The early biphasic kinetics of cofilin activity induced by PHEV entry were responsible for the mediation of F-actin assembly and disassembly. The PHEV-mediated early phosphorylation of cofilin involved integrin $\alpha5\beta1$-FAK signaling, which triggered events of F-actin recombination and viral entry. We also showed that PAKs were downstream regulators controlling cofilin activity and cell morphogenesis. Therefore, PHEV has evolved a complex mechanism of infecting N2a cells. Collectively, our results not only reveal the mechanism of actin rearrangement induced by PHEV infection but also provide new ideas for the development of new antiviral drugs.

RESULTS

PHEV infection induces N2a cells actin cytoskeletal remodeling. The changes in actin cytoskeleton of N2a cells caused by PHEV infection were assessed by confocal

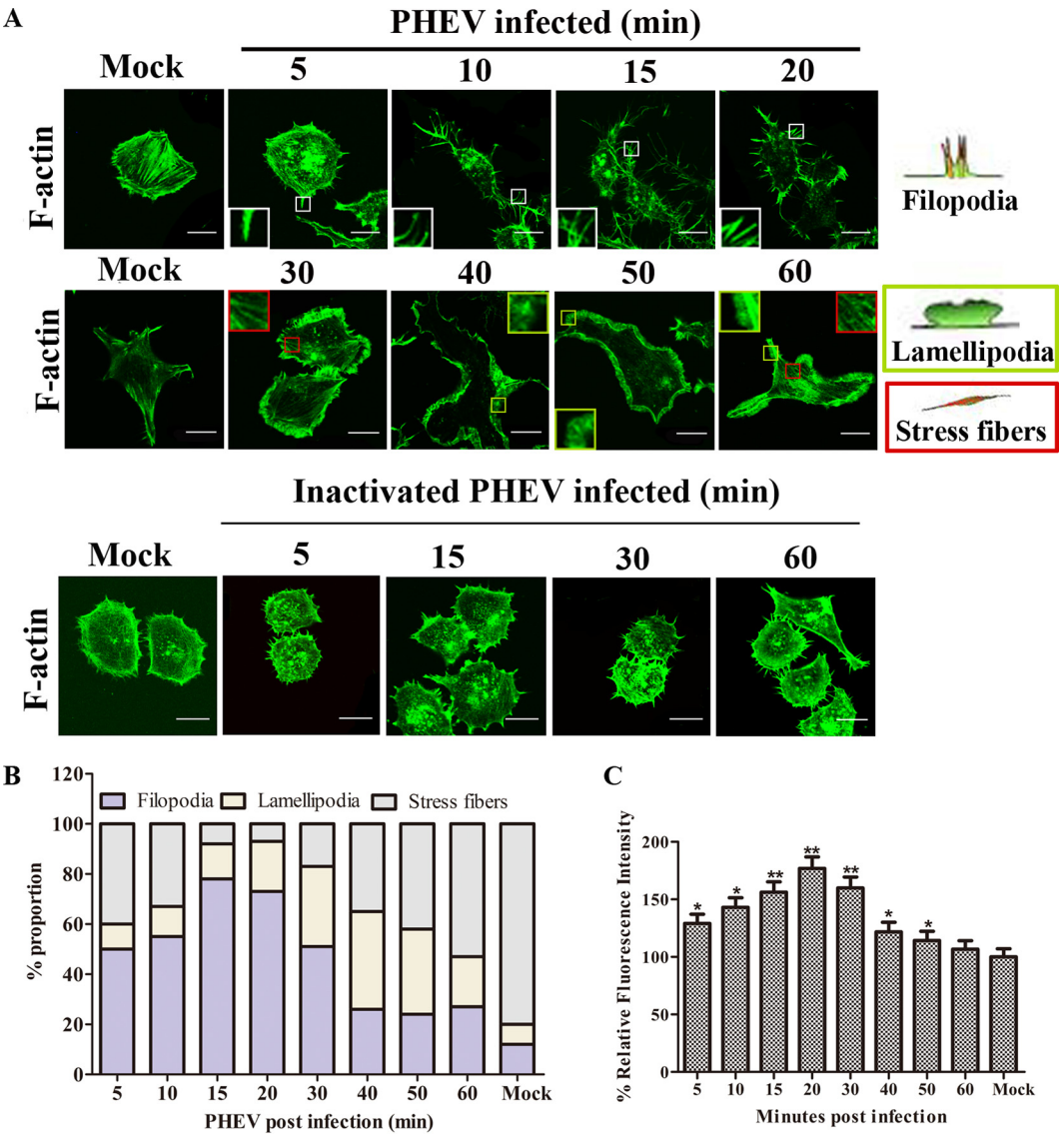

FIG 1 PHEV infection induces actin cytoskeletal remodeling. (A) PHEV infection induces cell protrusion formation. N2a cells were incubated with PHEV or inactivated PHEV (MOI of 50) for 1 h at 4°C and then moved to 37°C and fixed at the indicated time points. The untreated cells were used as a control (Mock). F-actin was stained with FITC-phalloidin (green) and observed by confocal microscopy. Scale bar, 10 μm. (B) Quantitative detection of cell ruffle changes at different time points after infection. Cells with F-actin stress fibers, lamellipodia, or filopodia were designated positive cells; each value represents the average value from 60 to 80 cells from at least 5 regions of 3 representative experiments. (C) PHEV treatment causes cell actin polymerization and depolymerization. F-actin was stained with FITC-phalloidin and analyzed by flow cytometry.

microscopy and staining with fluorescein isothiocyanate (FITC)-phalloidin. PHEV or inactivated PHEV was added to N2a cells at 4°C for 1 h to synchronize infection before the cells were transferred to 37°C to initiate infection, which is a method that has been widely used (23). Compared with inactivated virus and mock groups, we found that PHEV entry into N2a cells induced the formation of filopodia and lamellipodia or stress fibers at different times. As early as 5 min postinfection (mpi), we observed the dissolution of actin stress fibers and the appearance of filopodia and lamellipodia. However, stress fibers reappeared at 30 mpi (Fig. 1A). Simultaneously, we used ImageJ software to analyze the changes of actin semiquantitatively, which were consistent with the above-described results (Fig. 1B). The dynamic changes in F-actin caused by virus infection next were quantitatively determined by flow cytometry. F-actin showed rapid polymerization early (5 mpi) and then started depolymerization at 20 mpi (Fig. 1C).

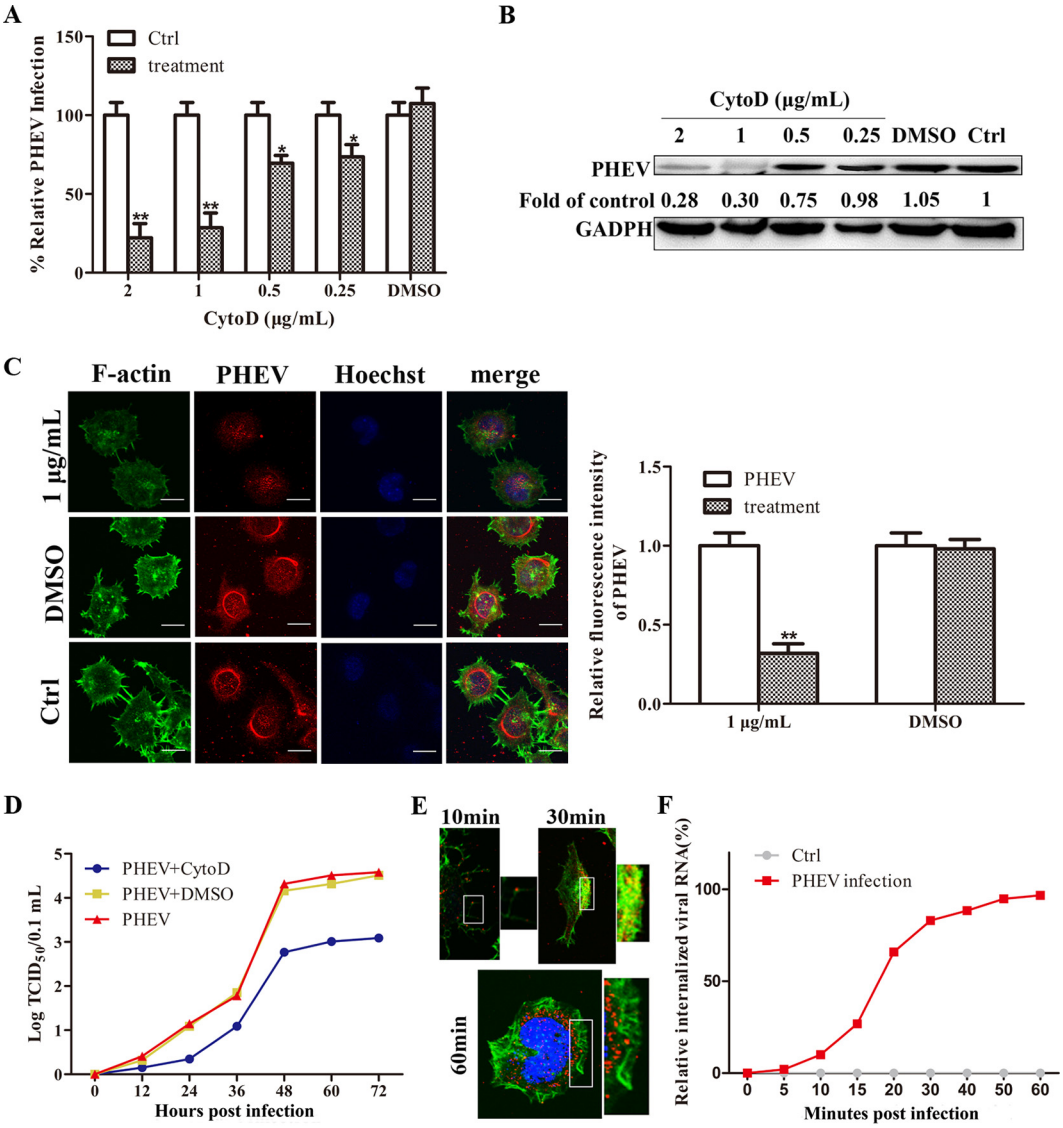

FIG 2 Inhibitors of F-actin inhibit virus entry. (A to C) CytoD inhibits the entry of PHEV in a concentration-dependent manner. Cells were pretreated with different concentrations of CytoD, and the internalization of PHEV was assessed using real-time PCR, Western blotting, and indirect immunofluorescence (see Materials and Methods). PHEV-infected cells were used as controls (Ctrl). DMSO, dimethylsulfoxide. (D) Growth analysis of PHEV. N2a cells were infected with PHEV after treatment with CytoD (1 μg/ml), and samples were collected at the indicated time points. Titers are expressed as $TCID_{50}$/0.1 ml. (E) Kinetics of PHEV entry into cells. Cells treated with PHEV were labeled with anti-S protein monoclonal antibody (red), FITC-phalloidin (green), and Hoechst (blue) at different time points. The figure shows the quantification of viral particle locations at different times. At least 30 cells from five representative fields were counted in each experiment. Scale bar, 10 μm. (F) PHEV bound to N2a cells at 4°C for 1 h were transferred to 37°C; at the indicated times, bound viral particles that did not enter the cells were removed, and internalized viral RNA was extracted and assayed by real-time PCR. All results were considered statistically significant at a P value of <0.05.

Actin cytoskeletal remodeling is crucial for PHEV invasion. Furthermore, we treated N2a cells with cytochalasin D (CytoD), which binds to and cleaves F-actin and binds at the ends of the filaments to impede the polymerization of actin at that site (23). Quantitative reverse transcription-PCR (qRT-PCR), Western blotting, and indirect immunofluorescence were used to detect the entry of PHEV. We observed that CytoD strongly disrupted actin polymerization after treatment of cells by confocal microscopy assay (Fig. 2C). Additionally, PHEV entry was impaired by the disruption of actin dynamics using CytoD and in a dose-dependent manner compared with entry in the control cells (Fig. 2A to C). Simultaneously, we also determined the growth kinetics of PHEV. Virus titer was significantly reduced after CytoD treatment (Fig. 2D). The rela-

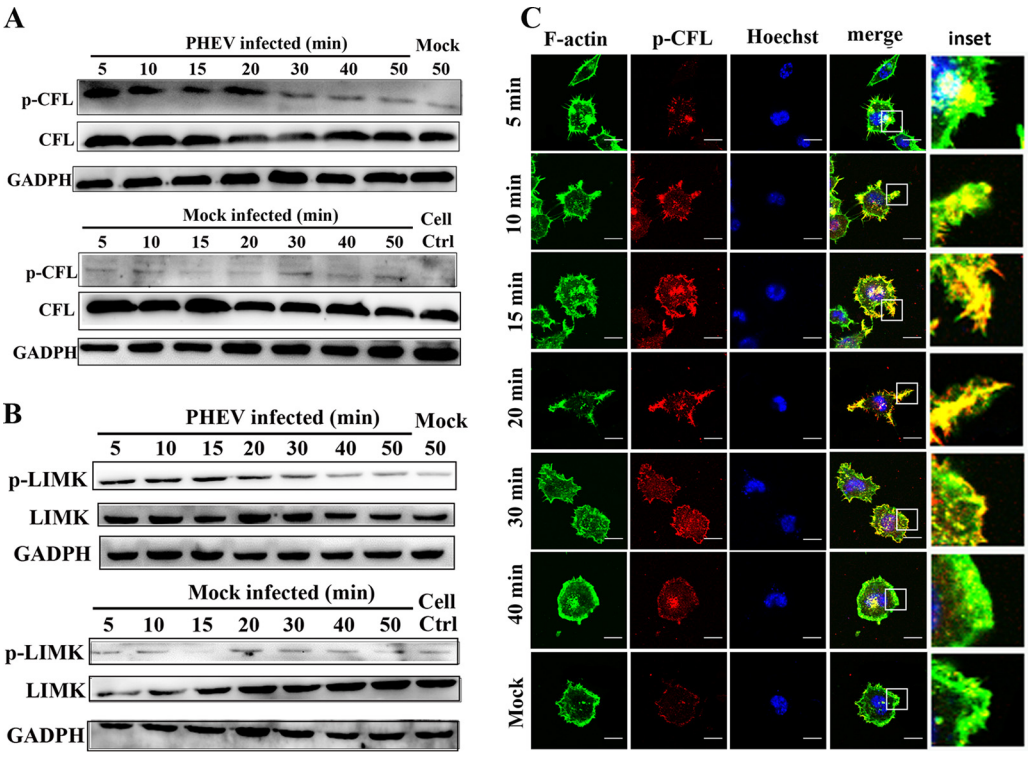

FIG 3 PHEV infection induces cofilin biphasic activation. (A) Cofilin activity test. Detection of cofilin phosphorylation with Western blotting at the designated times after infection. In all of the mock-infected experimental groups, the untreated cells were used as a control. In the PHEV-infected group, the cells that were incubated at 4°C for 1 h and then transferred to 37°C for the indicated times without PHEV infection to mimic infection were used as the control (Mock). (B) LIMK activity test. Detection of LIMK phosphorylation with Western blotting at the designated times after infection. (C) The level of p-cofilin increases early in PHEV infection. Cells treated with PHEV were labeled with anti-p-cofilin monoclonal antibody (red), FITC-phalloidin, and Hoechst at different time points. At least 30 cells from five representative fields were counted in each experiment. Scale bar, 10 μm.

tionship between PHEV particles and actin early in infection was further examined by confocal fluorescence microscopy, with infected cells stained using FITC-phalloidin and PHEV particles labeled with PHEV-S antibody. During the first 10 mpi, the virus primarily concentrated in the protuberances, such as filopodia; as the infection progressed, the virus particles moved along the filopodia to penetrate the membrane surface of the cell membrane, moving and distributing in the cell membrane surface (at 30 mpi); at 60 mpi, PHEV particles had almost completely entered the cytoplasm (Fig. 2E). Additionally, the kinetic curve of the virus entering the cell was determined by a fluorescence quantitative PCR method, as shown in Fig. 2F. The virus entry of the cell primarily occurred after 15 mpi. The results described above indicated that the entry of the virus is closely related to the dynamic changes of the cytoskeleton caused by the virus.

PHEV infection induces cofilin biphasic activation. The cellular actin cytoskeleton is regulated by cofilin, and the most important physiological function of cofilin is the cleavage and depolymerization of actin filaments to promote actin kinetics (4). Cofilin cannot bind to actin when phosphorylated, and activity is reactivated by dephosphorylation. LIMK and testicular protein kinase phosphorylate cofilin, whereas sphincter and chronophin phosphatase dephosphorylate cofilin (20). Because PHEV invasion of cells led to remodeling of the actin cytoskeleton, we examined the changes in cofilin activity during the viral infection. Western blotting showed that cofilin was first inactivated and then gradually activated after 30 mpi (Fig. 3A), which closely corresponded to the dynamic changes of F-actin, and a similar trend was also found by measuring the fluorescence intensity of cofilin (p-CFL) in the inactive state and its colocalization with F-actin (Fig. 3C). PHEV infection also induced transient activation of LIMK kinase early at 5 mpi, which was then inactivated at 30 mpi (Fig. 3B). Collectively, these results

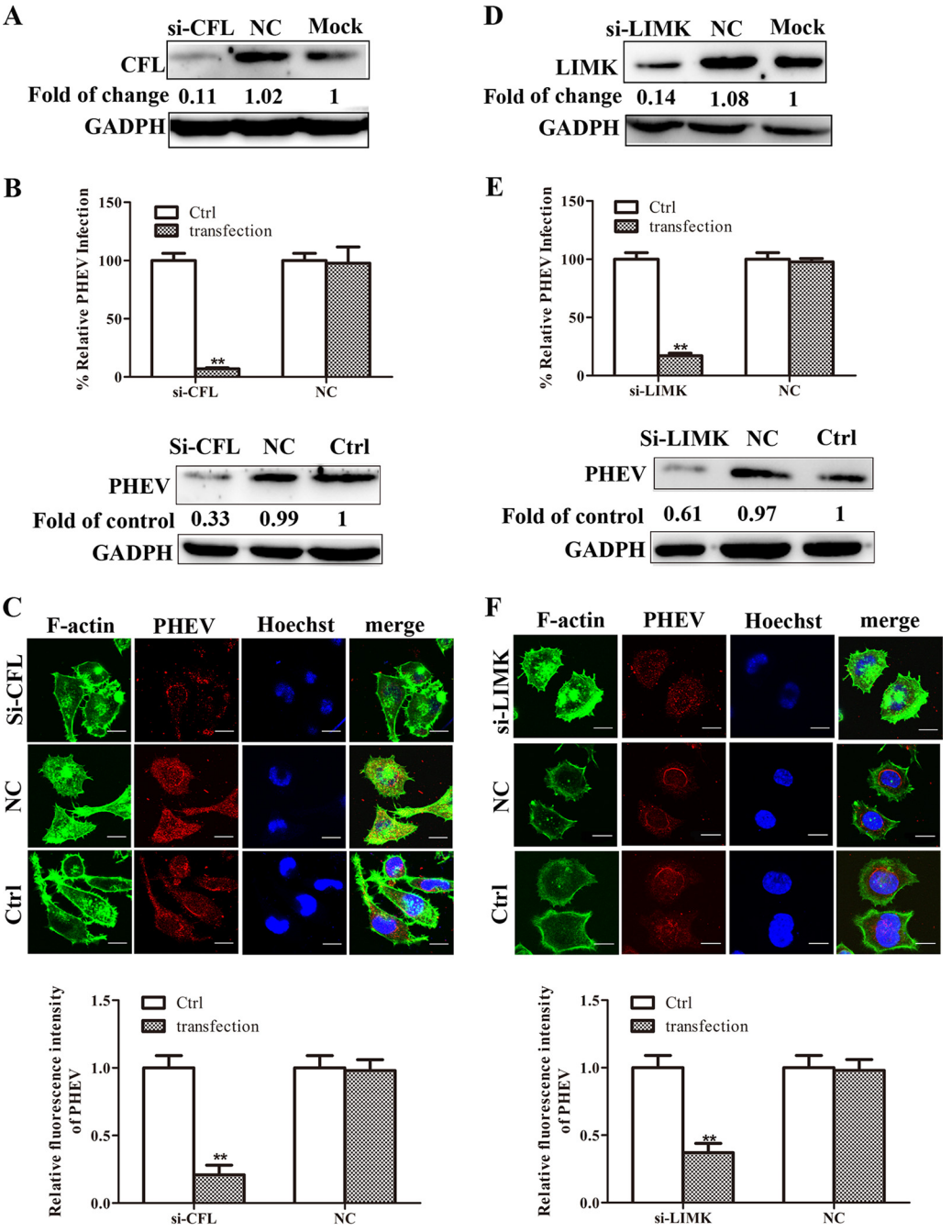

FIG 4 Cofilin and LIMK siRNAs affect viral entry. (A) Cofilin protein levels in N2a cells 24 h posttransfection with cofilin siRNA and siR-cofilin negative control (NC). (B and C) PHEV entry is inhibited when cofilin is knocked down. Cells were transfected with siRNA. Twenty-four hours after transfection, cells were infected with PHEV for 2 h, and PHEV entry was assessed by real-time PCR, Western blotting, and indirect immunofluorescence. Scale bar, 10 μm. (D) LIMK protein levels in N2a cells 24 h posttransfection with LIMK siRNA and siR-LIMK negative control (NC). (E and F) PHEV entry is inhibited when LIMK is knocked down. The same detection method was used as that for panel B. All results were considered statistically significant at a P value of <0.05.

showed that the regulation of cofilin activity mediated the dynamic changes of actin caused by the early infection of the virus.

Cofilin activity affects PHEV-induced actin cytoskeletal changes and viral entry. To confirm the role of cofilin in PHEV infection, we conducted a series of experiments and modulated cofilin activity by knockdown or overexpression. The virus entry process was significantly blocked at low expression of cofilin (Fig. 4A to C). Cofilin-specific short

interfering RNA (siRNA) inhibited cofilin expression approximately 90% according to Western blotting, qPCR, and indirect immunofluorescence, with the virus entering at only 30% of the level of control entry. LIMK-specific siRNA also inhibited PHEV entry (Fig. 4D to F).

Cells were also transfected with cofilin with a wild-type expression vector (WT), a constitutively unphosphorylated mutant cofilin (activated, S3A), or the constitutively phosphorylated mutant cofilin (inactivated, S3D). Notably, all three constructs inhibited PHEV entry in a dose-dependent manner, similar to the results of inhibition of cofilin expression (Fig. 5A). Additionally, PHEV entry particles were assessed by an immunofluorescence assay (IFA) using an anti-PHEV-S antibody. Detection by confocal microscopy showed that the virus entry process was reduced (Fig. 5B). Therefore, the dynamic phosphorylation of cofilin for the efficient entry of PHEV was essential. Cofilin may accumulate on cortical actin and participate in F-actin assembly and disassembly, which may affect viral binding and penetration. Additionally, cofilin-specific siRNAs could dilapidate cellular stress fibers, form small protrusions on the cell surface, and fragment actin filaments into lumps (Fig. 5C). These results indicated that cofilin is required for PHEV entry into cells and the maintenance of actin cytoskeletal stability. Additional microscopic experiments showed that peripheral migration of the virus on cells mobilized cofilin, and the strict control of local activity around the cofilin cells is crucial for virus entry (18). In the absence of PHEV stimulation, cofilin/WT expression and overexpression of mutant cofilin/S3A cells were positive for the cofilin rod-shaped structure. These rod-shaped structures were composed of active cofilin. Active cofilin can chelate actin, thereby reducing the production of wrinkles. These phenomena are consistent with increased cofilin activity (18). However, PHEV infection caused the rod-shaped structures to disappear, indicating that viral infection modulated cofilin activity (Fig. 5D). These observations suggested that alteration of cofilin activity favors viral adsorption and entry into cells.

Involvement of integrin $\alpha5\beta1$ in PHEV entry and cofilin phosphorylation. Cytoskeletal signaling molecules are usually mediated by G-protein-coupled receptors, lectins, and receptor tyrosine kinases (RTKs) in the regulation of cofilin activity. Additionally, several studies show that the virus binds to the cell surface receptor and induces an intracellular signaling cascade that is predominantly tyrosine phosphorylated. Therefore, we first examined whether RTKs were involved in virus entry and cofilin phosphorylation. When N2a cells were pretreated with genistein, a specific inhibitor of RTKs, viral entry and cofilin phosphorylation were not significantly affected (Fig. 6A and B). Therefore, RTKs were not involved in PHEV entry and cofilin phosphorylation. Integrins belong to the family of cell adhesion molecules and are a type of transmembrane protein widely found on the surface of animal and plant cell membranes. They are important regulatory factors in physiological activities such as cell migration and proliferation. Integrins consist of α and β subunits and exist as heterodimers on the cell surface (24). Integrin $\alpha5\beta1$ is a heterodimer composed of an $\alpha5$ subunit and $\beta1$ subunit. Integrin is an important receptor of fibronectin (FN) in the matrix and primarily mediates the interaction of cells with extracellular matrix proteins and plays an important role in cell motility, migration, and neural cell remodeling (25, 26). Therefore, we treated cells with the integrin $\alpha5\beta1$ inhibitor ATN-161 to determine whether integrin $\alpha5\beta1$ participated in PHEV entry into cells and cofilin phosphorylation. The results showed that viral entry and cofilin phosphorylation were significantly affected (Fig. 6C and D).

Additionally, integrin $\alpha5\beta1$ was significantly upregulated in the first 15 min of viral infection (Fig. 7A). The function of integrins depends on the rapid transformation of their own conformation (25, 26). Therefore, we speculate that the adsorption of the virus on the cell surface causes a change in the conformation of the integrin and initiates the integrin pathway. After the virus enters the cell, the conformation of the integrin is restored, that is, the integrin is activated during virus invasion. By confocal microscopy, we observed that the virus bound rapidly to induce integrin $\alpha5\beta1$ to relocate on the cell membrane when the virus entered the cell. Additionally, integrin

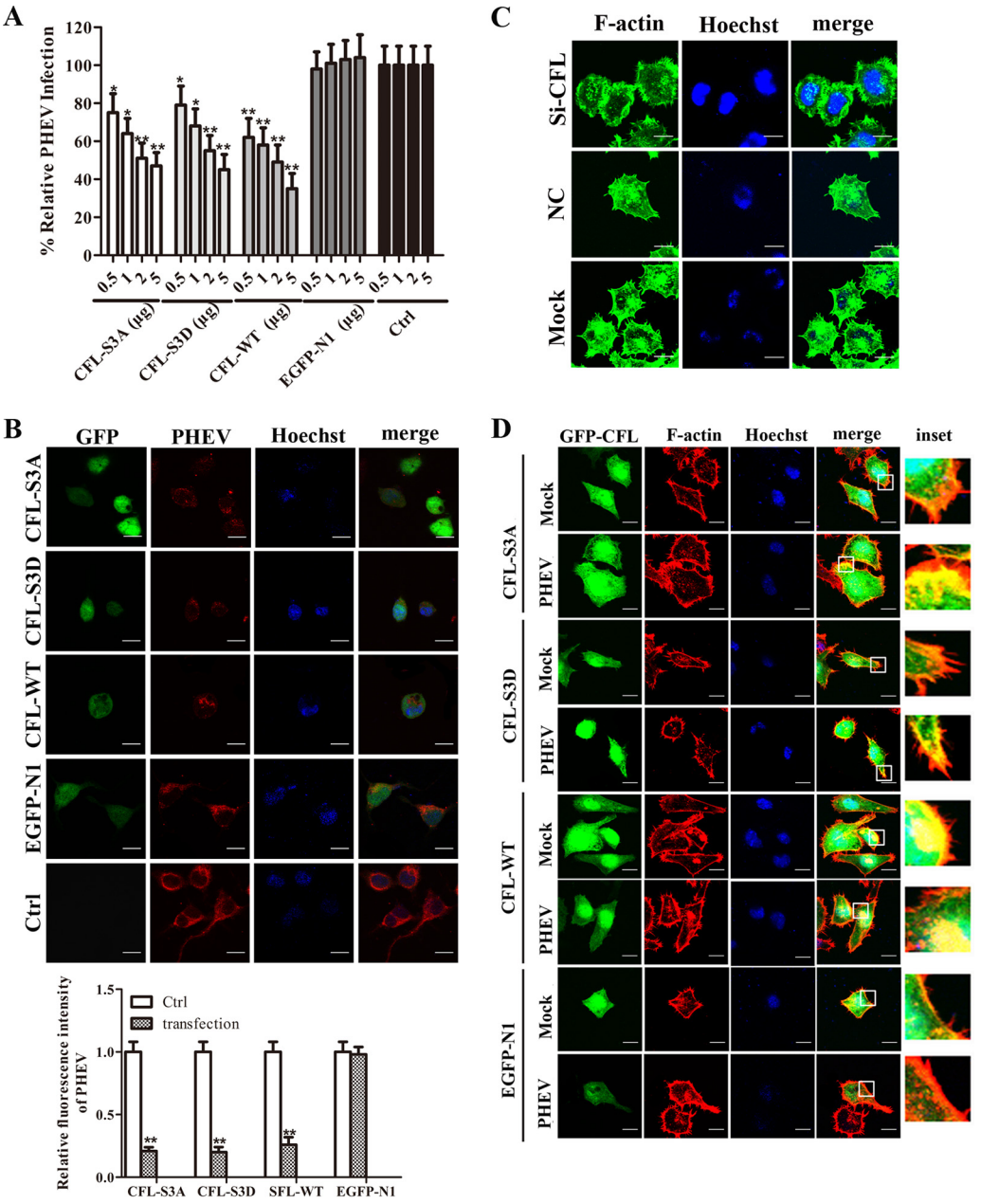

FIG 5 Cofilin activity influences virus entry and participates in virus-induced cell membrane ruffle formation. (A) Overexpression of wild-type cofilin or mutants (S3A and S3D) inhibits PHEV entry. The cells were transfected with plasmids (at different concentrations) and infected with PHEV for 2 h, and real-time PCR was used to detect PHEV entry. (B) Confocal microscopy showed overexpression of cofilin inhibited viral entry. Cells were transfected with green fluorescent protein (GFP)-tagged plasmids (2 μg) and then infected with PHEV for 2 h, fixed, and stained with anti-PHEV-S (red). In each independent experiment, at least 30 cells from five representative fields were counted. Scale bar, 10 μm. (C) Effects of cofilin siRNA on the actin cytoskeleton. Cells were fixed at 24 h after transfection with siRNA, F-actin was labeled with FITC-phalloidin, and nuclei were labeled with Hoechst, followed by observation with confocal microscopy. Scale bar, 10 μm. (D) Cofilin is involved in virus-induced cell protrusion formation. Cells were infected for 30 min, and then F-actin (red) or cofilin (green) was stained and examined by laser confocal microscopy. Scale bar, 10 μm. All results were considered statistically significant at a *P* value of <0.05.

$\alpha5\beta1$ was recruited to the virus entry site and colocalized with the virus S protein (Fig. 7B).

Integrin $\alpha5\beta1$ promotes PHEV entry into cells and PHEV-induced early cofilin phosphorylation through FAK signaling. FAK is a non-receptor tyrosine protein kinase that plays a key role in integrin-mediated signaling pathways (27). Therefore, we

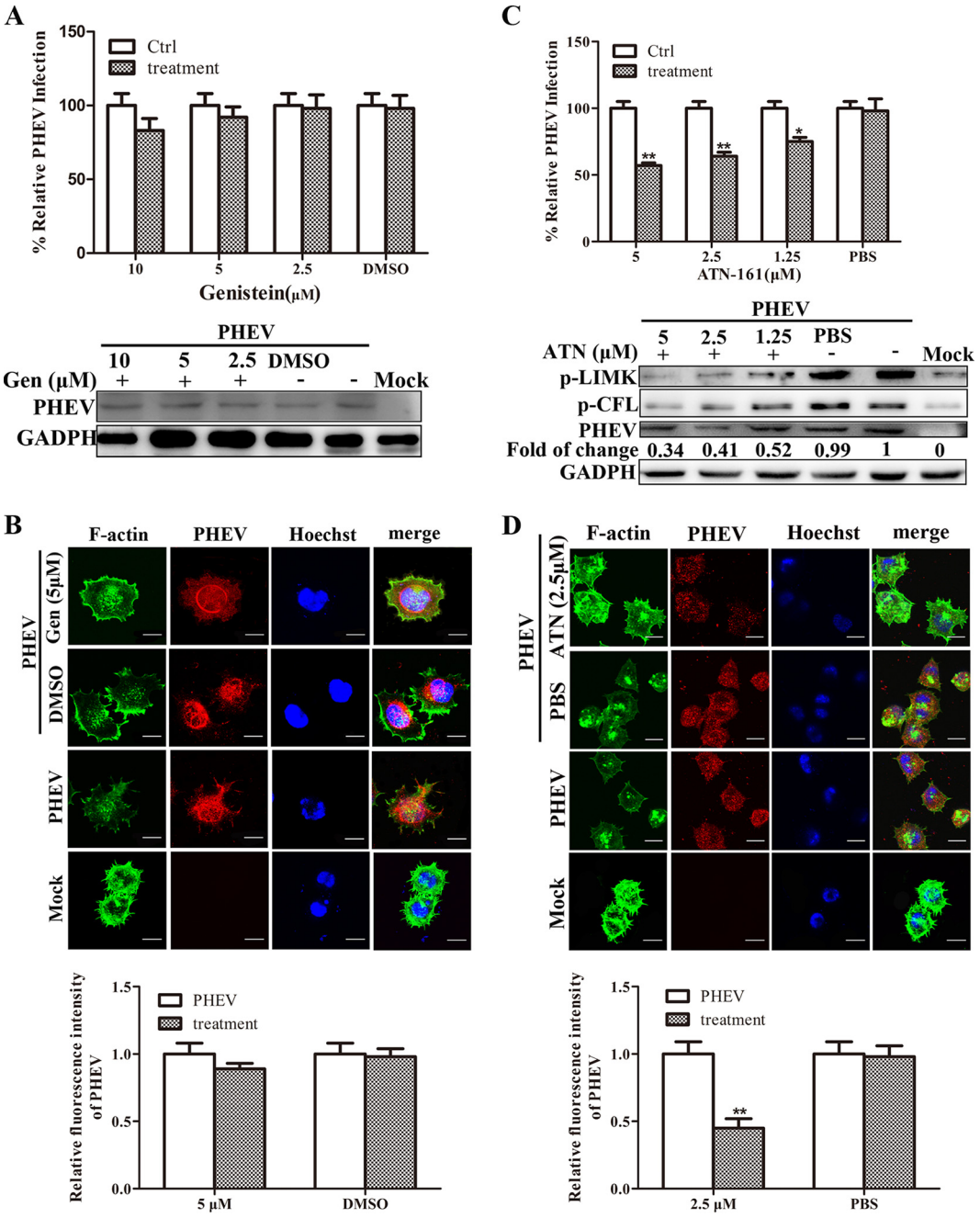

FIG 6 Integrins are involved in cofilin phosphorylation and viral entry. (A and B) RTKs are not involved in cofilin phosphorylation and virus entry. Cells were treated with different doses of genistein, an RTK specific inhibitor, at 37°C for 1 h and then infected with PHEV for 2 h. The internalization of PHEV was assessed by real-time PCR, Western blotting, and indirect immunofluorescence. (C and D) Integrin inhibitors inhibit viral entry and affect cofilin phosphorylation. Different doses of integrin $\alpha5\beta1$-specific inhibitor ATN-161 were used to treat cells at 37°C for 1 h. Cofilin and LIMK phosphorylation were detected by Western blotting, and the internalization of PHEV was assessed by real-time PCR, Western blotting, and indirect immunofluorescence. All results were considered statistically significant at a *P* value of <0.05.

tested whether PHEV infection activated FAK. Within 5 min, FAK was transiently activated when PHEV was added to the cells. FAK then was slowly inactivated and was almost completely inactivated in 20 min (Fig. 8A). This phenomenon was consistent with the cofilin phosphorylation period. These experiments suggested that FAK is associated with the process of PHEV entry into the cell and PHEV-induced early cofilin phosphorylation. To confirm this hypothesis, we treated cells with FAK-specific inhibitor PF-573228. The results showed that viral entry was significantly inhibited, and cofilin

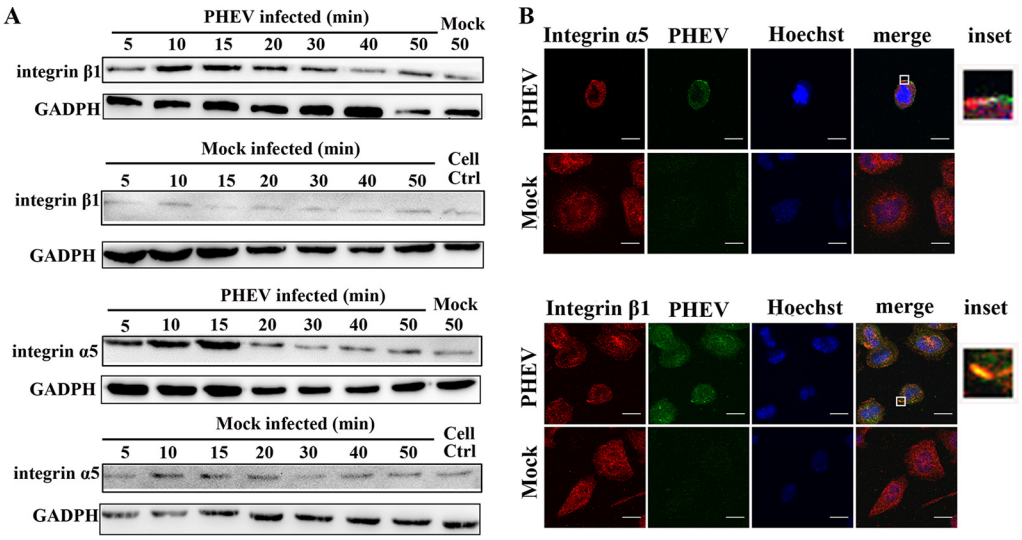

FIG 7 Integrin $\alpha5\beta1$ affects viral entry. Integrin $\alpha5\beta1$ expression is upregulated during PHEV entry. N2a cells were incubated with PHEV (MOI of 50) for 1 h at 4°C and then moved to 37°C and fixed at the indicated time points. Integrin $\alpha5\beta1$ was probed with integrin $\alpha5$ and integrin $\beta1$ antibodies. (B) Correlation of viral particles with integrin $\alpha5\beta1$ in infected cells. Cells were infected with PHEV for 15 min and then fixed, and indirect immunofluorescence assays were performed with anti-integrin $\alpha5/\beta1$ and anti-PHEV-S antibodies. Scale bar, 10 μm.

phosphorylation decreased in a concentration-dependent manner when the cells were inhibitor treated (Fig. 8B and C). Simultaneously, ATN-161 also affected FAK activation in PHEV infection early (Fig. 8D), which demonstrated the cellular processes of PHEV entry and PHEV-induced early cofilin phosphorylation involved FAK.

The FAK-centered integrin signaling pathway regulates two pathways; one is the Ras/mitogen-activated protein kinase (MAPK) pathway and the other is the FAK signaling pathway, which is independent of c-Src interaction. Activation of the Ras/MAPK pathway by FAK requires participation of Src (28). To verify which pathway is involved in PHEV-induced early cofilin phosphorylation, we performed the following experiments. The activation of Src in the early stage of PHEV infection was detected by Western blotting. The results showed that Src expression did not change and also was not activated in the early stages of PHEV infection (Fig. 8E). Additionally, pretreatment of N2a cells with PP2 (a specific inhibitor of Src family kinases) did not affect PHEV infection (Fig. 8F to G). Therefore, integrin $\alpha5\beta1$ promotes PHEV infiltration of cells and PHEV-induced early cofilin phosphorylation through the FAK signaling pathway, which is independent of c-Src interaction.

Rac1 and Cdc42 GTPases are involved in cofilin phosphorylation in PHEV infection early. The actin cytoskeleton is highly dynamic and is primarily manipulated by members of the Rho family of GTPases, which are activated by nucleotide exchange of bound GDP to GTP and can control signal transduction pathways that connect membrane receptors to the cytoskeleton (12). Rho family small G proteins are key proteins that regulate cell morphology and motility migration. These proteins regulate cell motility and cell morphology by controlling actin contraction and microtubule distribution (29). The three subfamilies RhoA, Rac, and Cdc42 regulate cell shape and migration through coordination (30). RhoA is responsible for the formation of stress fibers, Rac1 induces membrane ruffles or lamellipodia, and Cdc42 regulates the formation of protrusive filopodia (12). The FAK pathway can regulate cofilin phosphorylation by activating either Rac1 or Cdc42 (1). To study the role of Rac1 and Cdc42 GTPases early in the entry process of PHEV and PHEV-induced cofilin phosphorylation, we pretreated cells with Rac1 or Cdc42 GTPase inhibitors to determine whether they were upstream regulators of cofilin. Racl GTPase inhibitor EHoP-016 and Cdc42 GTPase inhibitor ML-141 both inhibited viral entry and affected cofilin phosphorylation during the early stages of PHEV infection (Fig. 9A to D).

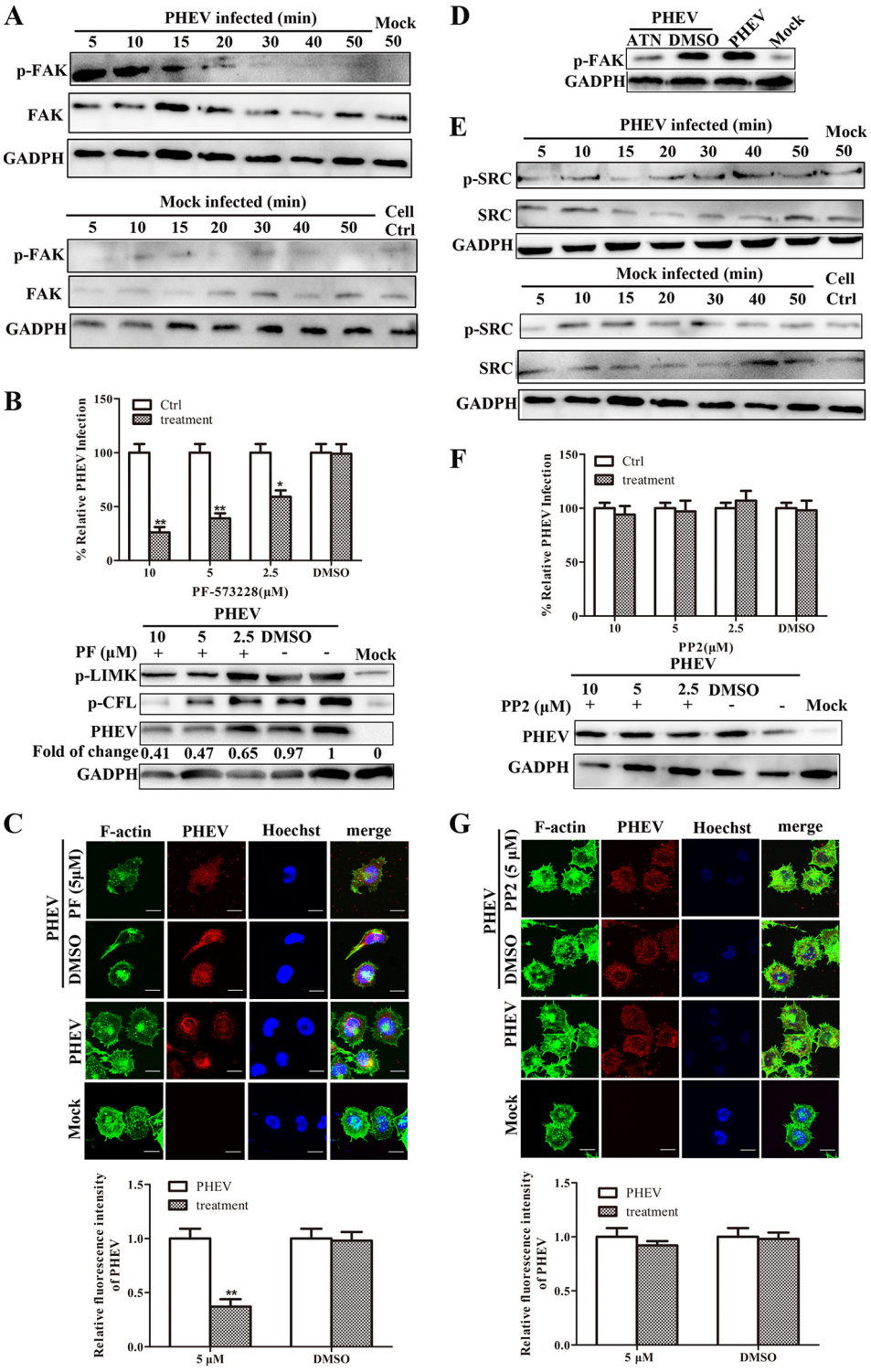

FIG 8 FAK is involved in cofilin phosphorylation and viral entry. (A) Activation of FAK during PHEV entry. PHEV-infected cell lysates were collected at different time points. Active FAK was probed with a p-FAK antibody. (B and C) FAK inhibitors inhibit viral entry and affect cofilin phosphorylation. Different doses of the FAK-specific inhibitor PF-573228 were used to treat cells at 37°C for 1 h and then infected with PHEV for 2 h. Cofilin and LIMK phosphorylation were detected by Western blotting, and the internalization of PHEV was assessed by real-time PCR, Western blotting, and indirect immunofluorescence. (D) Integrins are upstream proteins that regulate FAK activation. Cells were pretreated with ATN-161 (2.5 μM) for 1 h before infection. Ten minutes after PHEV infection, FAK phosphorylation levels of cell lysates were analyzed. (E to G) SRC is not involved in PHEV entry. Cells were treated with different doses of SRC-specific inhibitor PP2 at 37°C for 1 h and then infected with PHEV for 2 h. The internalization of PHEV was assessed by real-time PCR, Western blotting, and indirect immunofluorescence. All results were considered statistically significant at a P value of <0.05.

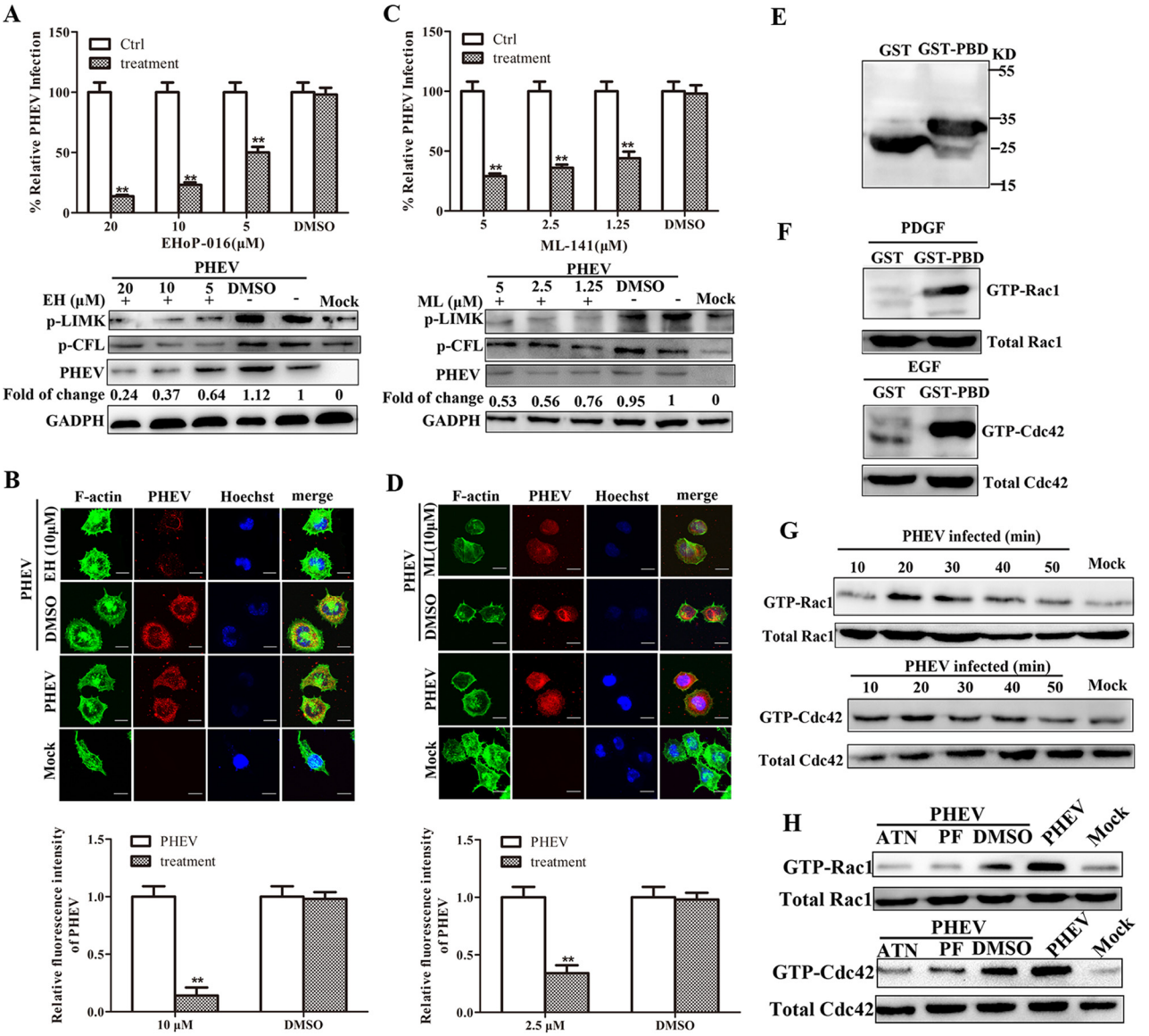

FIG 9 Rac1 GTPase and Cdc42 GTPase are involved in early cofilin phosphorylation and promote PHEV entry. (B) Rac GTPase specific inhibitor EHoP-016 (EH) affects viral entry and cofilin phosphorylation. Different doses of EHoP-016 were used to treat cells for 1 h, and then cofilin and LIMK phosphorylation were detected by Western blotting and the internalization of PHEV was assessed by real-time PCR, Western blotting, and indirect immunofluorescence. (C and D) ML-141 (ML), which is a Cdc42 GTPase-specific inhibitor, affects viral entry and cofilin phosphorylation. The same detection method was used as that for panels A and B. (E) GST-PBD protein purification. KD, molecular mass in kilodaltons. (F) GST-PBD specifically binds GTP-Rac1 and GTP-Cdc42. Lysates of cells that were treated with PDGF (20 ng/ml) or EGF (50 ng/ml) were incubated with GST-PBD. GST-PBD binds GTP-bound Rac1 and GTP-bound Cdc42 (pulldown), and total Rac1 and Cdc42 proteins in lysates were analyzed by Western blotting. (G) Rac1 and Cdc42 activation assay. Cells were harvested and lysed at different time points after PHEV treatment, and pulldown assays were performed as described above. (H) ATN-161 (2.5 μM) and PF-573228 (5 μM) affect Rac1 and Cdc42 activity. Cells were harvested and lysed after inhibitor treatment and virus inoculation for 20 min, and pulldown assays were performed as described above. All results were considered statistically significant at a P value of <0.05.

The small G proteins of the Rho family play a regulatory role by converting the GDP-bound inactive form to the GTP-bound activated form. To further examine the involvement of Rac1 and Cdc42 GTPases in PHEV-induced cofilin phosphorylation, we tested the activity of Rac1 and Cdc42 in the early stages of PHEV infection. According to the PAK1 protein p21 binding domain (PBD) with GTP-Rac1 and GTP-Cdc42 interaction principle (31), we detected the activation of Rac1 and Cdc42 by the glutathione *S*-transferase (GST) pulldown method. The PBD of PAK1 protein was constructed on a vector containing GST and expressed as a fusion protein (Fig. 9E). Platelet-derived growth factor (PDGF) and epidermal growth factor (EGF) significantly activated intra-

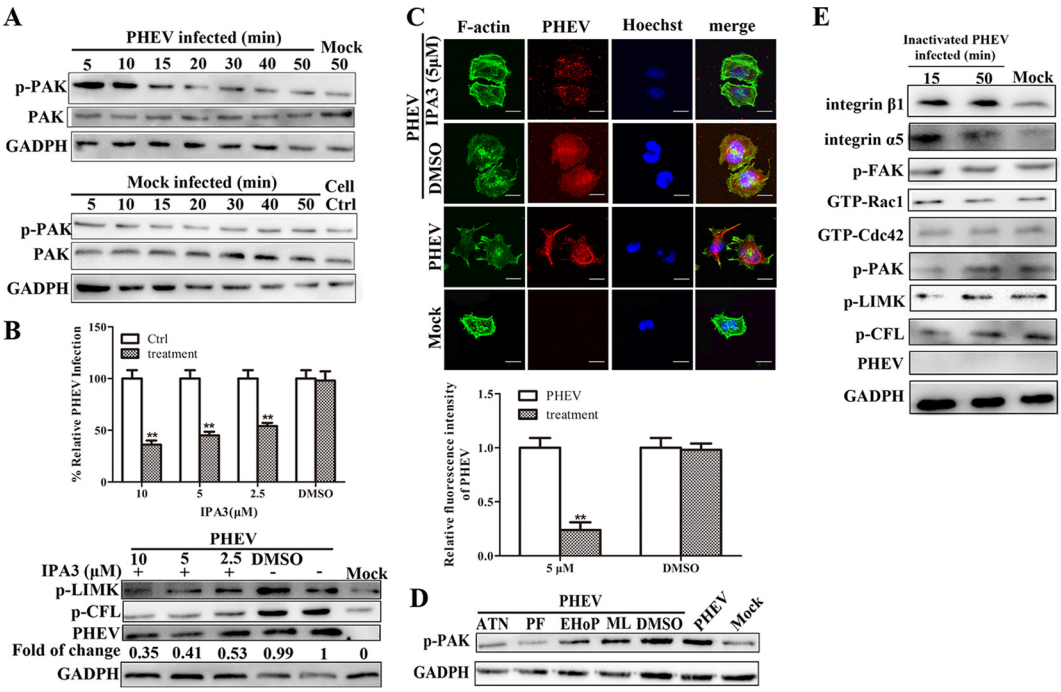

FIG 10 PAK is a downstream effector of PHEV-induced integrin $\alpha5\beta1$-FAK-Rac1/Cdc42 pathway in early cofilin phosphorylation. PAK is activated during PHEV entry. Cells were infected with PHEV, and cell lysates were analyzed with anti-PAK and anti-p-PAK antibodies. (B and C) PAK-specific inhibitor IPA3 affects viral entry and cofilin phosphorylation. Different doses of IPA3 were used to treat cells for 1 h, and then cofilin and LIMK phosphorylation were detected. (D) Inhibitors block the activation of PAK. Cells were pretreated with ATN-161 (2.5 μM), PF-573228 (5 μM), EHoP-016 (10 μM), or ML-141 (2.5 μM) for 1 h before infection. Ten minutes after PHEV infection, PAK phosphorylation levels of cell lysates were analyzed. (E) Integrin pathway was not activated in inactivated PHEV-infected N2a cells. N2a cells were incubated with inactivated PHEV (MOI of 50) for 1 h at 4°C and then moved to 37°C, and cells were harvested at the indicated time points. Detection of integrin pathway activation by Western blotting is shown. All results were considered statistically significant at a P value of <0.05.

cellular Rac1 and Cdc42, respectively (28, 32). The cells were treated with PDGF and EGF to test the specificity of the established method. The results showed that GST-PBD interacted with intracellularly activated Rac1 and Cdc42 and that this interaction was highly specific compared with that of the control group (Fig. 9F). The above-described method was used to detect the activation of Rac1 and Cdc42 at different time points after PHEV stimulation. As shown in Fig. 9G, Rac1 and Cdc42 were rapidly activated and slowly inactivated 20 min after viral infection, consistent with the dynamic changes of actins and the dynamic phosphorylation of cofilin. We also examined the effect of inhibitors of integrin $\alpha5\beta1$ and FAK on Rac1 and Cdc42 activity. Rac1 and Cdc42 activities were detected after cells were treated with inhibitors and inoculated with PHEV for 10 min. As shown in Fig. 9H, both integrin $\alpha5\beta1$ and FAK inhibitors affected Rac1 and Cdc42 activity induced by PHEV infection. The above-described results suggested that Rac1 and Cdc42 GTPases, as integrin $\alpha5\beta1$-FAK downstream kinases, regulate cofilin phosphorylation during the early phase of PHEV infection.

PAK1 is involved in cofilin phosphorylation as a downstream effector of Cdc42/Rac1. PAK1 is a Rho GTPase kinase that is closely related to the regulation of the cytoskeleton, which is activated by Rac1 or Cdc42 and can phosphorylate LIMK (33). We tested whether PAK1 was activated. In the early stages of virus infection, phosphorylation of PAK1 was obvious (Fig. 10A), and its inhibitor, IPA-3, had a significant effect on viral entry and cofilin phosphorylation (Fig. 10B and C). IPA3 also inhibited the generation of filopodia and lamellipodia that were caused by PHEV infection (Fig. 10C). Simultaneously, integrin $\alpha5\beta1$, FAK, Rac GTPase, and Cdc42 GTPase inhibitors reduced virus-induced PAK1 phosphorylation (Fig. 10D). Therefore, PAK1 acts as a downstream factor of the integrin $\alpha5\beta1$-FAK-Rac1/Cdc42 pathway to regulate the formation of protrusive filopodia and induce membrane ruffles or lamellipodia in the early stage of

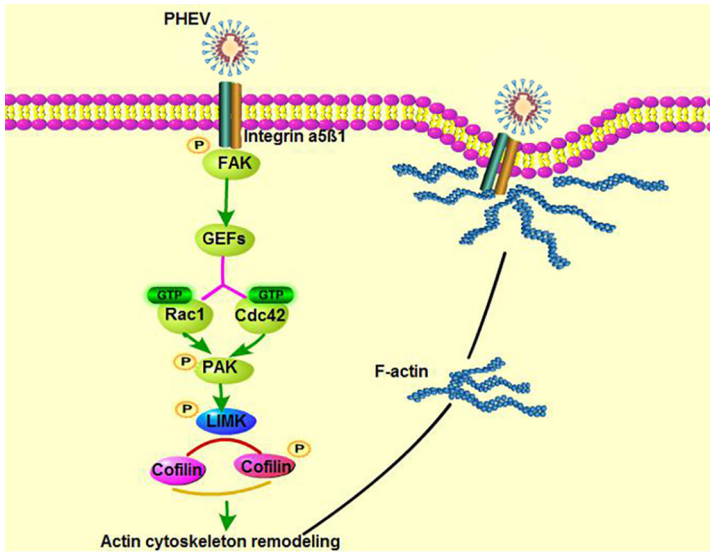

FIG 11 Model of cofilin regulating the actin cytoskeleton and initiating PHEV entry. In early stages of infection, PHEV stimulates the dynamic phosphorylation of cofilin and polymerizes F-actin via the integrin $\alpha5\beta1$-FAK-Rac1/Cdc42-PAK-LIMK signaling pathway.

PHEV infection. We then examined whether the pathway was activated in inactivated PHEV-inoculated cells. The results demonstrated that the pathway was not activated (Fig. 10E), indicating that the pathway activation required PHEV invasion.

DISCUSSION

Porcine hemagglutinating encephalomyelitis is an acute and highly contagious disease of pigs caused by PHEV, primarily affecting piglets less than 3 weeks of age, causing vomiting and wasting disease and significant neurological symptoms. Partly infected piglets have diarrhea symptoms (34–36). Currently, no effective prevention or treatment measures exist for this disease (37), which, when an outbreak occurs, causes enormous economic losses to the pig industry. Although the pathogenesis of PHEV and mechanisms of neural damage have been gradually characterized, very little research has been conducted on the pathways of virus entry into the cell. In this experiment, for the first time the cellular mechanism of PHEV cell entry was studied from the perspective of the actin cytoskeleton. The pattern is shown in Fig. 11. We determined that cofilin is a key factor required for PHEV infection. PHEV entry required a two-stage process of rapid polymerization and depolymerization of actin, and PHEV triggered bidirectional regulation of cofilin protein activity. Viral binding induced phosphorylation of cofilin by integrin $\alpha5\beta1$-FAK-Rac1/Cdc42-PAK-LIMK signaling for actin polymerization and efficient entry. Subsequent viral penetration activated cofilin, resulting in the fragmentation of existing actin filaments to promote viral trafficking. These findings suggested that PHEV promotes viral entry by regulating cofilin activity and inducing dynamic actin polymerization and depolymerization.

The cytoskeleton, which consists of microtubules, actin filaments, and intermediate filaments, plays an important role in many cellular functions, including cell structure, motility, signaling, and intracellular trafficking (38–40). Many viruses have developed mechanisms that allow them to exploit these structures to facilitate their replication (41). Actin filaments are composed of a polymer formed by G-actin monomers, namely, F-actin, and are primarily located in the cortical region below the cell membrane (42). Actin filaments play an important role in the maintenance of cell morphology and preventing the invasion of pathogens (11). A virus binds to its corresponding receptor on the extracellular matrix (ECM), and then the virus must migrate to sites that favor its particular entry pattern, either by direct plasma membrane fusion or by macrophage generation, phagocytosis, and various forms of clathrin-mediated and clathrin-indepen-

dent endocytosis (4). During this process, viruses often encounter actin rearrangement processes, such as filopodia and microvilli, and use these structures to efficiently move to the cell membrane (4). The rearrangement of the actin cytoskeleton induced by different types of viruses is different. For example, murine leukemia virus (MLV) must bind to receptors via the action of actin to form a virus-receptor complex and move to a suitable location for the virus to complete endocytosis (43). Herpes simplex virus 1 (HSV-1) requires the simultaneous polymerization and depolymerization of actin filaments to complete its binding to host cells (44). Poliovirus also utilizes the actin- and tyrosine kinase-dependent pathways into the cell (45). All of these results indicate that viruses utilize the complexity and diversity of host cell actin. In our previous research, PHEV entered neural cells primarily through clathrin-mediated endocytosis, and for this process to be completed, an acidic environment with the participation of various proteins was required, including proteins such as mobilized proteins, cholesterol, and Eps15. Simultaneously, actin cytoskeleton integrity is positively correlated with virus endocytosis during PHEV invasion (22), but the role and mechanism of the actin cytoskeleton in this process are not clear. In this study, we observed actin rearrangements with the formation of cellular filopodia and lamellipodia and the solubilization of actin stress fibers and their repositioning around the cell membrane in the early stages of PHEV infection. Additionally, the virus moves along the filopodia to the cell membrane. Cofilin is involved in neurodegenerative diseases as one of the actin filament regulatory factors (18). Cofilin activity is also involved in virus-mediated actin remodeling (2). In the early stages of PHEV infection, we also found that cofilin dynamic phosphorylation was the key to the virus effectively entering cells. The dynamic regulation of cofilin activity mediates the formation of cellular processes caused by viruses, and the critical control of local cofilin activity is crucial for actin-dependent processes such as receptor aggregation and intracellular migration.

Many regulatory mechanisms that affect the activity of cofilin in host cells are caused by viral infection, with effects on RTKs, integrins, and other pathways. RTKs can convert extracellular signals into intracellular signals and regulate the structure of the actin cytoskeleton (46). Integrins are heterodimers formed by the different pairings of 18 α and 8 β subunits. Integrins provide a link between the ECM protein and the actin cytoskeleton, which is critical for the regulation of the cytoskeleton and intracellular signaling pathways. Additionally, integrins participate in the process of virus entry into cells (47). Most viruses affect the rearrangement of the actin cytoskeleton of host cells through RTK signaling pathways, such as transmissible gastroenteritis virus (TGEV), porcine reproductive and respiratory syndrome virus (PRRSV), and HSV-1 (47). However, our results showed that PHEV affected actin cytoskeleton rearrangement and cofilin activity via the integrin $\alpha5\beta1$-FAK signaling pathway. Integrin $\alpha5\beta1$ not only accumulated at the PHEV attachment but also promoted the activation of FAK, which is a downstream kinase. Additionally, integrin $\alpha5\beta1$ inhibitor ATN-161 blocked PHEV infection by inhibiting the downstream signaling cascade. Many viruses use integrins and related rafts to promote binding and internalization, consolidating the role of integrins in virus internalization and infection (3) and suggesting that internalization of integrins is a common mechanism by which a virus enters the cell. Notably, we also found another difference between PHEV and most other viruses in this experiment, such as hepatitis B virus (HBV), Ebola virus (EBOV), and infectious bursal disease virus (IBDV) (48–50): the Src kinase did not participate in the process of virus-induced actin cytoskeleton rearrangement and did not affect cofilin activity. Src kinase is a member of the cytoplasmic tyrosine kinase family and participates in a variety of signal transduction pathways in the cell (50). Under normal physiological conditions, FAK activates and then activates the Src family kinase under the action of integrin (51). FAK was activated during PHEV entry into host cells, but Src phosphorylation levels did not change. Additionally, the process of PHEV entry into the cell was not affected after treatment with Src-specific inhibitors. These results demonstrated that PHEV regulates actin cytoskeleton rearrangements using the FAK signaling pathway independent of the Src family.

Actin rearrangement requires the regulation of the upstream Rho GTPase family, of which the most important are Rac1, Cdc42, and RhoA. In this study, we found that PHEV invasion of N2a cells was dependent on the roles of Rac1 and Cdc42. Additionally, we also demonstrated that Rac1 and Cdc42 were downstream Rho GTPases of the integrin $\alpha5$ $\beta1$-FAK pathway, and both Rac1 and Cdc42 affected the rearrangement of the actin cytoskeleton by regulating the activity of cofilin through downstream PAK molecules. PAK is an evolutionarily conserved serine/threonine protein kinase whose phosphorylation promotes the formation of actin filaments through the inactivation of cofilin; the dephosphorylation restores the interaction between cofilin molecules and actin monomers, which depolymerizes actin filaments. This regulatory process affects the rearrangement of the actin cytoskeleton (6). Although both Rac1 and Cdc42 regulated the actin cytoskeleton rearrangement through PAK, we found that the activation time of Rac1 and Cdc42 in PHEV invasion of N2a cells was different. In the stage of virus invasion, the activation of Cdc42 was earlier than that of Rac1. Whether different activation times of Rho GTPases indicate different roles requires further exploration.

Collectively, our results identified specific mechanisms of cytoskeletal remodeling during PHEV entry into N2a cells, which could provide a theoretical basis for a better understanding of the pathogenesis of PHEV-induced neurological symptoms and for the study of new antiviral drugs. We emphasize the role of cofilin activity regulation as a molecular switch to provide a link between cytoskeletal remodeling and viral entry processes. Therefore, cofilin and upstream signaling molecules are viable targets for development of therapeutic antiviral strategies.

MATERIALS AND METHODS

Cell lines. N2a cells were maintained in Dulbecco's modified Eagle's medium (DMEM) (Gibco, Grand Island, NY) with high glucose containing 10% fetal calf serum (Biological Industries, Israel), 1% streptomycin, and 1% penicillin incubated at 37°C in a wetted chamber supplemented with 5% CO_2.

Virus and infection. The strain used in this experiment was PHEV 67 N (GenBank accession no. AY078417), which was propagated in N2a cells and stored at −80°C until use. We inactivated the virus by incubation for 24 h at 37°C. For assays on the entry of PHEV, cells were incubated with PHEV at a multiplicity of infection (MOI) of 50 for 1 h at 4°C, washed with phosphate-buffered saline (PBS; pH 7.2 at 4°C) three times to remove unbound virus, and then maintained in DMEM supplemented with 2% FBS and 1% penicillin-streptomycin at 37°C in a 5% CO_2 incubator. After the indicated time, cells were washed with PBS (pH 7.2 at 4°C) to remove the viruses bound to the cell membrane, and then TRIzol or radioimmunoprecipitation assay (RIPA) lysis buffer was added to collect samples or 4% paraformaldehyde was used to treat cells. The entry of PHEV was determined by qRT-PCR, confocal microscopy (FV10-ASW 3.0, 522; Olympus Europa Holding, GmbH) with the anti-PHEV-S antibody, and Western blotting. For experiments involving inhibitor stimulation, cells were pretreated with inhibitors for 1 h, PHEV was added, and the procedure was performed as described above.

Virus growth analysis. N2a cell monolayers in 6-well plates were pretreated with CytoD for 1 h and incubated with PHEV for 1 h at 4°C. Cells were washed three times with PBS to remove unbound virus and then maintained in DMEM. One hundred μl of sample was harvested from the cell supernatant at various time points, and virus titers were quantified on N2a cells.

Antibodies, small-compound inhibitors, and siRNAs. Antibodies against cofilin, phospho-cofilin, integrin $\alpha5$, integrin $\beta1$, FAK, phospho-FAK, Src, phospho-Src, Rac1, and Cdc42 were purchased from Cell Signaling Technology (Beverly, MA). Antibodies against RhoA, PAK1, and phospho-PAK1 were purchased from Abcam (Cambridge, UK). Antibodies against LIMK1 and phospho-LIMK1 were purchased from BIOSS (Beijing, China). Glyceraldehyde-3-phosphate dehydrogenase (GAPDH) antibody, horseradish peroxidase (HRP)-linked secondary anti-rabbit or anti-mouse IgG antibodies, Cy3-conjugated AffiniPure goat anti-rabbit IgG (H+L) secondary antibodies, and Cy3- or FITC-conjugated AffiniPure goat anti-mouse IgG (H+L) secondary antibodies were purchased from Proteintech (Chicago, IL). Mouse anti-PHEV-S antibody was a laboratory-prepared monoclonal antibody. FITC-phalloidin was purchased from Cytoskeleton (Denver, CO). CytoD and genistein were purchased from Sigma (St. Louis MO, USA). All specific inhibitors, ATN-161, PF-573228, PP2, EHoP-016, ML-141, and IPA3 were purchased from Selleck (Houston, TX, USA). All inhibitors were used at a noncytotoxic concentration. The cytotoxicity of chemical inhibitors was determined with a cell-counting kit. The cofilin siRNA target sequence was GGATCAAGCATGAATTGCA AGCAAA. The LIM domain kinase 1 siRNA target sequence was GAATGTGGTGGTGGCTGAC.

RNA extraction and qRT-PCR. Total RNA from N2a cells infected with PHEV was extracted using TRIzol reagent (Invitrogen, Gaithersburg, MD) according to the manufacturer's instructions. The cDNA was generated by reverse transcription using PrimeScript reverse transcriptase (TaKaRa, Japan) according to the manufacturer's instructions. PHEV entry was assessed based on detection of the viral spike protein gene using qRT-PCR with a TaKaRa SYBR green qPCR kit (TaKaRa, Japan) on a CFX96 Touch real-time PCR detection system (Bio-Rad, USA). Primer sequences were the following: PHEV sense primer, 5′-AGCGAT GAGGCTATTCCGACTA-3′; antisense primer, 5′-TTGCCAGAATTGGCTCTACTACG-3′; mouse GAPDH sense

primer, 5′-CTCAACTACATGGTCTACATGTTC-3′; antisense primer, 5′-ATTTGATGTTAGTGGGGTCTCGCTC-3′. PCR products were purified using a gel extraction kit and cloned into the pMD18-T vector (TaKaRa, Japan). Plasmids were diluted serially and used as standards for quantitative analysis. The initial copy number of PHEV S gene and GAPDH in each group was calculated using the formula $X = -K \log(C_T + b)$, where X is the initial copy number and K, C_T, and b refer to the slope rate, cycle threshold, and constant, respectively.

Western blotting. At indicated times of infection, cells were washed three times with PBS and lysed for 30 min in RIPA buffer (1% Triton X-100 and 1 mM phenylmethylsulfonyl fluoride [PMSF] in PBS) on ice. The concentration of protein was determined using a bicinchoninic acid (BCA) protein assay kit (Thermo Scientific, USA). The protein samples (50 mg/lane) were separated using 10% polyacrylamide gels and were transferred to 0.22-μm polyvinylidene fluoride membranes using the Bio-Rad wet transfer system. After blocking for 1 h at 37°C with 5% nonfat dry milk in PBS and reacting with the indicated primary antibodies at 4°C overnight, membranes were exposed to species-specific HRP-conjugated secondary antibodies followed by enhanced chemiluminescence (ECL; Thermo Scientific, USA) detection by autoradiography. GAPDH was used as a loading control.

Plasmid construction and transfection. pEGFP-cofilin-WT, pEGFP-cofilin-S3A (a nonphosphorylatable mutant), and pEGFP-cofilin-S3D (a phosphomimetic mutant) were constructed as described in the literature (52). Plasmid transfection was performed using X-tremeGENE HP DNA transfection reagent (Roche, Sweden) according to the manufacturer's instructions. For the RNA interference assay, N2a cells were transfected with siRNA using X-tremeGENE siRNA transfection reagent (Roche, Sweden) according to the manufacturer's instructions, and the knockdown efficiencies were quantified by RT-PCR and Western blotting. Subsequent experiments were performed 24 h after transfection.

Immunofluorescence staining and confocal microscopy. N2a cells were plated in 12-well plates with coverslips at a density of 1×10^4 cells/well in DMEM containing 10% fetal bovine serum and were grown overnight. Cells were incubated with PHEV at an MOI of 50 for 1 h at 4°C and then shifted to 37°C. At the indicated time points, cells were washed with PBS, fixed with 4% paraformaldehyde for 15 min at room temperature, and then permeabilized with 0.2% Triton X-100 for 15 min and blocked with 5% nonfat milk powder for 1 h at 37°C. To stain actin, FITC-phalloidin was added to samples for 30 min at 37°C, which were then washed with PBS and incubated overnight at 4°C with primary antibodies, i.e., anti-p-cofilin (1:100), anti-integrin α5 (1:100), anti-integrin β1 (1:100), and anti-PHEV (1:200). After washing with PBS three times, the FITC-conjugated AffiniPure goat anti-mouse IgG (H+L), Cy3-conjugated AffiniPure goat anti-mouse IgG (H+L), or Cy3-conjugated AffiniPure goat anti-rabbit IgG (H+L) secondary antibody (Proteintech) was incubated with PBS at 37°C for 1 h. Hoechst was used to stain the nuclei. After washing with PBS three times, the coverslips were mounted onto glass with antifade solution (Solarbio) before visualization on a confocal microscope. All images were acquired randomly using a laser scanning confocal fluorescence microscope (Olympus FluoView FV1000). The number of viruses entered and subcellular colocalization were analyzed by ImageJ and MATLAB software.

Pulldown assay for activated CDC42 and RAC1. The Rac1 and Cdc42 binding domains (PBDs) of PAK1 were first cloned into a plasmid encoding the fusion protein GST-PBD in *Escherichia coli* BL21 in pGEX-4T-1 and treated with 0.1 mM isopropyl-β-D-thiogalactopyranoside (IPTG) to induce expression. GST-PBD was then affinity purified using glutathione Sepharose 4B beads (Amersham Pharmacia Biotech) and quantified by SDS-PAGE. Cells were harvested and lysed after PDGF or EGF treatment of cells, at different time points after PHEV treatment, or 10 min after inhibitor treatment and virus inoculation. Cell lysates were centrifuged at 120,000 rpm for 15 min at 4°C. The supernatant was incubated with purified GST-PBD protein on a rotary mixer overnight at 4°C. After washing three times, the lysis buffer and the corresponding volume of 5× loading buffer were added into the EP tube and boiled for 10 min, followed by detection of the target protein by Western blotting.

Cytotoxicity assay. N2a cells were plated in 96-well plates at a density of 2×10^4 cells/well in DMEM containing 10% fetal bovine serum and were grown overnight. Cells then were treated with inhibitors at the indicated concentrations for 1 h. After two washes with PBS, 10 μl of the CKC-8 solution was added to 100 μl of DMEM in each well of a 96-well plate and incubated at 37°C for 1 h. The absorbance was measured at 450 nm with a microplate reader. None of the concentrations of chemicals used in this experiment resulted in significant cytotoxic effects on cell viability.

Image and statistical analyses. Values are presented as the arithmetic means ± standard errors. Each experiment was repeated at least 3 times. The SPSS 17.0 statistical software package (Chicago, IL) was used to analyze all data. Histograms were prepared with GraphPad Prism 5.0 software (San Diego, CA, USA). Western blot pictures were analyzed by Tanon Gis software (Shanghai, China). All results were considered statistically significant at a P value of <0.05.

ACKNOWLEDGMENTS

This study was supported by the National Key Research and Development Program of China (grant 2016YFD0500102), the National Natural Science Foundation of China (grants 31872446, 31772704, 31672519, and 31602018), and the Scientific and Technological Project of Jilin Province (grants 20180101270JC, 20170204033NY, and 20160520033JH). The funders had no role in study design, data collection and interpretation, or the decision to submit the work for publication. We declare that we have no conflicts of interest.

X.L. and W.H. designed and supervised the experiments. X.L. and Z.L. performed

most of the experiments and interpreted the data. J.G., S.H., and J.Z. cultured neurons, analyzed the confocal laser scanning images, made ultrathin sections, and analyzed them by transmission electron microscopy. Y.L. and H.H. constructed plasmids. K.Z., H.L., and D.S. carried out the coimmunoprecipitation test and prepared the figures and tables. F.G. supervised the experiments and interpreted some data. X.L. drafted the article, and W.H. revised it critically for important intellectual content.

REFERENCES

1. Spear M, Wu Y. 2014. Viral exploitation of actin: force-generation and scaffolding functions in viral infection. Virol Sin 29:139–147. https://doi.org/10.1007/s12250-014-3476-0.
2. MacLeod IJ, Minson T. 2010. Binding of herpes simplex virus type-1 virions leads to the induction of intracellular signalling in the absence of virus entry. PLoS One 5:e9560. https://doi.org/10.1371/journal.pone.0009560.
3. Salameh S, Sheth U, Shukla D. 2012. Early events in herpes simplex virus lifecycle with implications for an infection of lifetime. Open Virol J 6:1–6. https://doi.org/10.2174/1874357901206010001.
4. Wurth MA, Schowalter RM, Smith EC, Moncman CL, Dutch RE, McCann RO. 2010. The actin cytoskeleton inhibits pore expansion during PIV5 fusion protein-promoted cell-cell fusion. Virology 404:117–126. https://doi.org/10.1016/j.virol.2010.04.024.
5. Foo KY, Chee HY. 2015. Interaction between flavivirus and cytoskeleton during virus replication. Biomed Res Int 2015:427814. https://doi.org/10.1155/2015/427814.
6. Koga R, Sugita Y, Noda T, Yanagi Y, Ohno S. 2015. Actin-modulating protein cofilin is involved in the formation of measles virus ribonucleoprotein complex at the perinuclear region. J Virol 89:10524–10531. https://doi.org/10.1128/JVI.01819-15.
7. Belouzard S, Millet JK, Licitra BN, Whittaker GR. 2012. Mechanisms of coronavirus cell entry mediated by the viral spike protein. Viruses 4:1011–1033. https://doi.org/10.3390/v4061011.
8. Ding N, Zhao K, Lan Y, Li Z, Lv X, Su J, Lu H, Gao F, He W. 2017. Induction of atypical autophagy by porcine hemagglutinating encephalomyelitis virus contributes to viral replication. Front Cell Infect Microbiol 7:56. https://doi.org/10.3389/fcimb.2017.00056.
9. Li Z, Lan Y, Zhao K, Lv X, Ding N, Lu H, Zhang J, Yue H, Shi J, Song D, Gao F, He W. 2017. miR-142-5p disrupts neuronal morphogenesis underlying porcine hemagglutinating encephalomyelitis virus infection by targeting Ulk1. Front Cell Infect Microbiol 7:155. https://doi.org/10.3389/fcimb.2017.00155.
10. Lv X, Zhao K, Lan Y, Li Z, Ding N, Su J, Lu H, Song D, Gao F, He W. 2017. miR-21a-5p contributes to porcine hemagglutinating encephalomyelitis virus proliferation via targeting CASK-interactive protein1 in vivo and vitro. Front Microbiol 8:304. https://doi.org/10.3389/fmicb.2017.00304.
11. Grove J, Marsh M. 2011. The cell biology of receptor-mediated virus entry. J Cell Biol 195:1071–1082. https://doi.org/10.1083/jcb.201108131.
12. Taylor MP, Koyuncu OO, Enquist LW. 2011. Subversion of the actin cytoskeleton during viral infection. Nat Rev Microbiol 9:427–439. https://doi.org/10.1038/nrmicro2574.
13. Freeman MC, Peek CT, Becker MM, Smith EC, Denison MR. 2014. Coronaviruses induce entry-independent, continuous macropinocytosis. mBio 5:e01340-14. https://doi.org/10.1128/mBio.01340-14.
14. Clement C, Tiwari V, Scanlan PM, Valyi-Nagy T, Yue BY, Shukla D. 2006. A novel role for phagocytosis-like uptake in herpes simplex virus entry. J Cell Biol 174:1009–1021. https://doi.org/10.1083/jcb.200509155.
15. Min S, Lim YS, Shin D, Park C, Park JB, Kim S, Windisch MP, Hwang SB. 2017. Abl tyrosine kinase regulates hepatitis C virus entry. Front Microbiol 8:1129. https://doi.org/10.3389/fmicb.2017.01129.
16. Delorme-Axford E, Coyne CB. 2011. The actin cytoskeleton as a barrier to virus infection of polarized epithelial cells. Viruses 3:2462–2477. https://doi.org/10.3390/v3122462.
17. Popow-Woźniak A, Mazur AJ, Mannherz HG, Malicka-Błaszkiewicz M, Nowak D. 2012. Cofilin overexpression affects actin cytoskeleton organization and migration of human colon adenocarcinoma cells. Histochem Cell Biol 138:725–736. https://doi.org/10.1007/s00418-012-0988-2.
18. Mizuno K. 2013. Signaling mechanisms and functional roles of cofilin phosphorylation and dephosphorylation. Cell Signal 25:457–469. https://doi.org/10.1016/j.cellsig.2012.11.001.
19. Hussein HA, Walker LR, Abdel-Raouf UM, Desouky SA, Montasser AK, Akula SM. 2015. Beyond RGD: virus interactions with integrins. Arch Virol 160:2669–2681. https://doi.org/10.1007/s00705-015-2579-8.
20. Kim JY, Wang L, Lee J, Ou JJ. 2017. Hepatitis C virus induces the localization of lipid rafts to autophagosomes for its RNA replication. J Virol 91:e00541-17.
21. Zheng X, Liu W, Xiang J, Liu P, Ke M, Wang B, Wu R, Lv Y. 2017. Collagen I promotes hepatocellular carcinoma cell proliferation by regulating integrin β1/FAK signaling pathway in nonalcoholic fatty liver. Oncotarget 8:95586–95595. https://doi.org/10.18632/oncotarget.21525.
22. Li Z, Zhao K, Lan Y, Lv X, Hu S, Guan J, Lu H, Zhang J, Shi J, Yang Y, Song D, Gao F, He W. 2017. Porcine hemagglutinating encephalomyelitis virus enters Neuro-2a cells via clathrin-mediated endocytosis in a Rab5-, cholesterol-, and pH-dependent manner. J Virol 91:e01083-17.
23. Zheng K, Xiang Y, Wang X, Wang Q, Zhong M, Wang S, Wang X, Fan J, Kitazato K, Wang Y. 2014. Epidermal growth factor receptor-PI3K signaling controls cofilin activity to facilitate herpes simplex virus 1 entry into neuronal cells. mBio 5:e00958-13. https://doi.org/10.1128/mBio.00958-13.
24. Wu X, Muthuchamy M, Reddy DS. 2017. Atomic force microscopy investigations of fibronectin and alpha5beta1-integrin signaling in neuroplasticity and seizure susceptibility in experimental epilepsy. Epilepsy Res 138:71–80. https://doi.org/10.1016/j.eplepsyres.2017.10.013.
25. Ehrlicher AJ, Nakamura F, Hartwig JH, Weitz DA, Stossel TP. 2011. Mechanical strain in actin networks regulates FilGAP and integrin binding to filamin A. Nature 478:260–263. https://doi.org/10.1038/nature10430.
26. Wu X, Reddy DS. 2012. Integrins as receptor targets for neurological disorders. Pharmacol Ther 134:68–81. https://doi.org/10.1016/j.pharmthera.2011.12.008.
27. Vitillo L, Kimber SJ. 2017. Integrin and FAK regulation of human pluripotent stem cells. Curr Stem Cell Rep 3:358–365. https://doi.org/10.1007/s40778-017-0100-x.
28. Hernández AJA, Reyes VL, Albores-García D, Gómez R, Calderón-Aranda ES. 2018. MeHg affects the activation of FAK, Src, Rac1 and Cdc42, critical proteins for cell movement in PDGF-stimulated SH-SY5Y neuroblastoma cells. Toxicology 394:35–44. https://doi.org/10.1016/j.tox.2017.11.019.
29. Lawson CD, Ridley AJ. 2017. Rho GTPase signaling complexes in cell migration and invasion. J Cell Biol 217:447–457. https://doi.org/10.1083/jcb.201612069.
30. Dada O, Gutowski S, Brautigam CA, Chen Z, Sternweis PC. 2017. Direct regulation of p190RhoGEF by activated Rho and Rac GTPases. J Struct Biol https://doi.org/10.1016/j.jsb.2017.11.014.
31. Larson Y, Liu J, Stevens PD, Li X, Li J, Evers BM, Gao T. 2010. Tuberous sclerosis complex 2 (TSC2) regulates cell migration and polarity through activation of CDC42 and RAC1. J Biol Chem 285:24987–24998. https://doi.org/10.1074/jbc.M109.096917.
32. Wang XY, Gan MX, Li Y, Zhan WH, Han TY, Han XJ, Cheng JQ, Wang JB. 2015. Cdc42 induces EGF receptor protein accumulation and promotes EGF receptor nuclear transport and cellular transformation. FEBS Lett 589:255–262. https://doi.org/10.1016/j.febslet.2014.11.049.
33. Vorster PJ, Guo J, Yoder A, Wang W, Zheng Y, Xu X, Yu D, Spear M, Wu Y. 2011. LIM kinase 1 modulates cortical actin and CXCR4 cycling and is activated by HIV-1 to initiate viral infection. J Biol Chem 286:12554–12564. https://doi.org/10.1074/jbc.M110.182238.
34. Chen K, He W, Lu H, Song D, Gao W, Lan Y, Zhao K, Gao F. 2011. Development of an immunochromatographic strip for serological diagnosis of Porcine hemagglutinating encephalomyelitis virus. J Vet Diagn Invest 23:288–296. https://doi.org/10.1177/104063871102300214.
35. Gao W, Zhao K, Zhao C, Du C, Ren W, Song D, Lu H, Chen K, Li Z, Lan Y, Xie S, He W, Gao F. 2011. Vomiting and wasting disease associated with hemagglutinating encephalomyelitis viruses infection in piglets in Jilin, China. Virol J 8:130. https://doi.org/10.1186/1743-422X-8-130.
36. Li Z, He W, Lan Y, Zhao K, Lv X, Lu H, Ding N, Zhang J, Shi J, Shan C, Gao F. 2016. The evidence of porcine hemagglutinating encephalomyelitis

virus induced nonsuppurative encephalitis as the cause of death in piglets. PeerJ 4:e2443. https://doi.org/10.7717/peerj.2443.
37. Lan Y, Zhao K, Wang G, Dong B, Zhao J, Tang B, Lu H, Gao W, Chang L, Jin Z, Gao F, He W. 2013. Porcine hemagglutinating encephalomyelitis virus induces apoptosis in a porcine kidney cell line via caspase-dependent pathways. Virus Res 176:292–297. https://doi.org/10.1016/j.virusres.2013.05.019.
38. Bogatcheva NV, Verin AD. 2008. The role of cytoskeleton in the regulation of vascular endothelial barrier function. Microvasc Res 76:202–207. https://doi.org/10.1016/j.mvr.2008.06.003.
39. Herrmann H, Strelkov SV, Burkhard P, Aebi U. 2009. Intermediate filaments: primary determinants of cell architecture and plasticity. J Clin Investig 119:1772–1783. https://doi.org/10.1172/JCI38214.
40. Nogales E. 2000. Structural insights into microtubule function. Annu Rev Biochem 69:277–302. https://doi.org/10.1146/annurev.biochem.69.1.277.
41. Leopold PL, Pfister KK. 2006. Viral strategies for intracellular trafficking: motors and microtubules. Traffic 7:516–523. https://doi.org/10.1111/j.1600-0854.2006.00408.x.
42. De Conto F, Fazzi A, Razin SV, Arcangeletti MC, Medici MC, Belletti S, Chezzi C, Calderaro A. 2017. Mammalian Diaphanous-related formin-1 restricts early phases of influenza A/NWS/33 virus (H1N1) infection in LLC-MK2 cells by affecting cytoskeleton dynamics. Mol Cell Biochem 437:185–201. https://doi.org/10.1007/s11010-017-3107-9.
43. Lehmann MJ, Sherer NM, Marks CB, Pypaert M, Mothes W. 2005. Actin- and myosin-driven movement of viruses along filopodia precedes their entry into cells. J Cell Biol 170:317–325. https://doi.org/10.1083/jcb.200503059.
44. Dixit R, Tiwari V, Shukla D. 2008. Herpes simplex virus type 1 induces filopodia in differentiated P19 neural cells to facilitate viral spread. Neurosci Lett 440:113–118. https://doi.org/10.1016/j.neulet.2008.05.031.
45. Brandenburg B, Lee LY, Lakadamyali M, Rust MJ, Zhuang X, Hogle JM. 2007. Imaging poliovirus entry in live cells. PLoS Biol 5:e183. https://doi.org/10.1371/journal.pbio.0050183.
46. Menard L, Parker PJ, Kermorgant S. 2014. Receptor tyrosine kinase c-Met controls the cytoskeleton from different endosomes via different pathways. Nat Commun 5:3907. https://doi.org/10.1038/ncomms4907.
47. LaFoya B, Munroe JA, Miyamoto A, Detweiler MA, Crow JJ, Gazdik T, Albig AR. 2018. Beyond the matrix: the many non-ECM ligands for integrins. Int J Mol Sci 19:E449.
48. Liu W, Guo TF, Jing ZT, Yang Z, Liu L, Yang YP, Lin X, Tong QY. 2018. Hepatitis B virus core protein promotes hepatocarcinogenesis by enhancing Src expression and activating the Src/PI3K/Akt pathway. FASEB J 32:3033–3046. https://doi.org/10.1096/fj.201701144R:fj201701144R.
49. Furuyama W, Marzi A, Carmody AB, Maruyama J, Kuroda M, Miyamoto H, Nanbo A, Manzoor R, Yoshida R, Igarashi M, Feldmann H, Takada A. 2016. Fcgamma-receptor IIa-mediated Src signaling pathway is essential for the antibody-dependent enhancement of Ebola virus infection. PLoS Pathog 12:e1006139. https://doi.org/10.1371/journal.ppat.1006139.
50. Ye C, Han X, Yu Z, Zhang E, Wang L, Liu H. 2017. Infectious bursal disease virus activates c-Src to promote alpha4beta1 integrin-dependent viral entry by modulating the downstream Akt-RhoA GTPase-actin rearrangement cascade. J Virol 91:e01891-16.
51. Naranatt PP, Akula SM, Zien CA, Krishnan HH, Chandran B. 2003. Kaposi's sarcoma-associated herpesvirus induces the phosphatidylinositol 3-kinase-PKC-MEK-ERK signaling pathway in target cells early during infection: implications for infectivity. J Virol 77:1524–1539. https://doi.org/10.1128/JVI.77.2.1524-1539.2003.
52. Lu Y, Cao L, Egami Y, Kawai K, Araki N. 2016. Cofilin contributes to phagocytosis of IgG-opsonized particles but not non-opsonized particles in RAW264 macrophages. Microscopy (Oxf) 65:233–242. https://doi.org/10.1093/jmicro/dfv376.